A Progressive Translational Mouse Model of Human VCP Disease: The VCP $^{R155H/+}$ Mouse

Angèle Nalbandian, PhD[1,*], **Katrina J. Llewellyn, PhD**[1,*], **Mallikarjun Badadani, PhD**[1], **Hong Z. Yin, MD**[2], **Christopher Nguyen, BS**[1], **Veeral Katheria, BS**[1], **Giles Watts, PhD**[4], **Jogeshwar Mukherjee, PhD**[3], **Jouni Vesa, PhD**[1], **Vincent Caiozzo, PhD**[5], **Tahseen Mozaffar, MD**[2,5], **John H. Weiss, MD**[2], and **Virginia E. Kimonis, MD, MRCP**[1,#]

[1]Department of Pediatrics, Division of Genetics and Metabolism, 2501 Hewitt Hall, University of California-Irvine, Irvine, CA 92697, USA

[2]Department of Neurology, Gillespie Hall, University of California-Irvine, Irvine, CA 92697, USA

[3]Preclinical Imaging Center, Department of Radiological Sciences, Medical Science C, University of California-Irvine, Irvine, CA 92697, USA

[4]Cell Biology and Biochemistry, School of Medicine, Health Policy and Practice, Biomedical Research Centre, University of East Anglia, Norwich, Norfolk, UK

[5]Department of Orthopedics, University of California-Irvine, Irvine, CA, 92697, USA

Abstract

Introduction—Mutations in the valosin containing protein (VCP) gene cause hereditary Inclusion Body Myopathy (hIBM) associated with Paget disease of bone (PDB), and frontotemporal dementia (FTD). More recently they have been linked to 2% of familial ALS cases. A knock-in mouse model offers the opportunity to study VCP-associated pathogenesis.

Methods—The VCP$^{R155H/+}$ knock-in mouse model was assessed for muscle strength, immunohistochemical, Western, apoptosis, autophagy and MicroPET/CT imaging analyses.

Results—VCP$^{R155H/+}$ mice developed significant progressive muscle weakness, and the quadriceps and brain developed progressive cytoplasmic accumulation of TDP-43, ubiquitin-positive inclusion bodies and increased LC3-II staining. MicroCT analyses revealed Paget-like lesions at the ends of long bones. Spinal cord demonstrated neurodegenerative changes, ubiquitin, and TDP-43 pathology of motor neurons.

Discussion—VCP$^{R155H/+}$ knock-in mice represent an excellent pre-clinical model for understanding VCP-associated disease mechanisms and future treatments.

Keywords

Amyotrophic Lateral Sclerosis (ALS); Inclusion Body Myopathy; Paget Disease of Bone; Frontotemporal Dementia (IBMPFD); Valosin Containing Protein (VCP); molecular genetics, pathology

[#]CORRESPONDENCE: Virginia Kimonis, MDProfessor, Department of Pediatrics, University of California, Irvine, Division of Genetics and Metabolism, Department of Pediatrics, 2501 Hewitt Hall, Irvine, CA 92696, Tel: (714) 456-5791, Direct: (714) 456-2942, Fax: (714) 456-5330, Pager: (714) 506-2063 vkimonis@uci.edu .
[*]Co-first authors of manuscript

Conflict of Interest Disclosures/Competing Interests
The authors have no personal financial or institutional interest or conflicts in any of the drugs, materials, or devices as described in this article.

INTRODUCTION

Inclusion body myopathy associated with Paget disease of bone and frontotemporal dementia (IBMPFD, OMIM 167320) is a multisystem degenerative disease due to mutations in the valosin containing protein (*VCP*) gene [1-2]. The myopathy occurs at a mean age of 42 years in 80-90% of patients. It is typically proximal and involving the pelvic and shoulder girdle muscles with progression to other muscle groups [13-4]. At later stages of the disease, the weakness involves respiratory muscles, leading to death from respiratory and cardiac failure. The pathology of inclusion body myopathy is manifested by rimmed vacuoles and inclusion bodies in muscle fibers [1-25], and the accumulated inclusion bodies are positive for TAR DNA binding protein-43 (TDP-43) and ubiquitin [6]. Abnormal vacuolization and increased Light Chain 3 (LC3) of patient myoblasts and autophagosome development suggests impaired autophagy [7]. In view of the shared TDP pathology [8], it is not surprising that Amyotrophic Lateral Sclerosis (ALS) is seen in approximately 10-15% of individuals with VCP disease. ALS is a neurodegenerative disease which involves both upper and lower motor neuron degeneration, and motor symptoms progressively spread to other anatomical regions [9]. Recently, VCP mutations have been linked to 2% of isolated familial amyotrophic lateral sclerosis (ALS) by Johnson et al. who studied 28 familial, 210 isolated ALS cases [10], and 0.5% of sporadic cases of ALS [11]. However, in 2 independent studies by Williams et al. (2011) and Tiloca et al. (2012) in which they explored VCP mutation and frequency analyses in large fALS patient cohorts, VCP was not the main causative gene for ALS [12-13]. Paget disease of bone (PDB) occurs in 49% and has an early onset in the 30s to 40s (mean 42 years) in patients compared to the general population [14-5]. PDB is caused by overactive osteoclastic activity resulting in pain, bony deformities, fractures and occasionally osteosarcomas. PDB typically affects the skull, vertebral column, pelvis and hip [314]. Diagnosis of PDB is established upon findings of elevated concentrations of serum alkaline phosphatase (ALP), elevated collagen cross-linkers in the urine, typical skeletal radiography findings, or hot spots on radionuclide scans [14].

Premature frontotemporal dementia (FTD) is observed in 27% of patients at a mean age of onset of 57 years [15]. FTD is a degenerative condition affecting primarily the frontal and anterior temporal lobes. [16-18] It is characterized by comprehension deficits, dysnomia, dyscalculia, relative preservation of memory, paraphrasic errors and social unawareness [5]. Affected individuals typically die in their 40s to 50s from progressive myopathy and associated cardiac and respiratory failure. FTD typically accelerates the progression of the disease.

VCP is a member of the type II AAA (ATPases associated with diverse cellular activities) possessing two ATPase domains [19]. VCP plays a critical role in a broad range of cellular activities, including homotypic membrane assembly, the ubiquitin-proteasome system (UPS), endoplasmic reticulum associated degradation of proteins (ERAD), cell cycle regulation, and DNA repair, preventing polyglutamine aggregation, autophagosome maturation and mitophagy [20-21]. However, the precise mechanism of how *VCP* mutations result in the pathogenesis of IBMPFD remains unclear. Mutations of VCP are most frequently within the N-terminal domain, which is involved in ubiquitin-binding and protein-protein interactions [222]. The mutated residues alter the orientation of the VCP domains and the relative three-dimensional orientations, and thus interfere with the interactions between VCP and its substrates [23]. VCP disease is being recognized more frequently with over 20 mutations having been identified worldwide [24]. The R155H mutation is by far the most common mutation, accounting for approximately 50% of affected individuals [225-26].

Transgenic mouse models provide an opportunity to understand the *in vivo* effects of VCP mutations and the pathogenesis of IBMPFD, since the mouse VCP differs from the corresponding human protein by one residue [27]. Deletion of the *VCP* gene in homozygous mutant mice resulted in early embryonic lethality, and hemizygotes that lack one *VCP* allele were found to be indistinguishable from their wild-type littermates [28]. Transgenic over-expression of the R155H mutation under the regulation of the muscle creatinine kinase promoter in mice revealed progressive muscle weakness beginning at the age of 6 months, and muscle pathology beginning at the age of 10 months included variation in muscle fiber size, increase in endomysial connective tissue, small linear basophilic-rimmed cracks, and ubiquitin-positive sarcoplasmic and myonuclear vacuoles [29]. Custer et al. generated transgenic mice that ubiquitously over-expressed mutant forms of VCP which exhibited characteristic inclusion body myopathy with muscle weakness and with blue-rimmed vacuoles on histology [30]. Paget-like bone disease with focal lytic and sclerotic regions was seen. Widespread TDP-43 brain pathology and abnormalities in behavioral testing were observed [29-30].

We have generated a Neomycin cassette-free novel *VCP*$^{R155H/+}$ knock-in mouse as a true model of the disease, which expresses the mutant *VCP* allele at an endogenous level ~~without interference from the Neomycin cassette.~~ The *VCP*$^{R155H/+}$ mouse model demonstrates muscle weakness, typical histopathology, and progressive accumulation of TDP-43, ubiquitin, and LC3 in muscle, resembling the onset in humans in the 30s-40s. The *VCP*$^{R155H/+}$ mice show milder, but typical muscle and brain pathology and mild increases in TDP-43, ubiquitin, and LC3 pathology. Additionally, the spinal cords of these animals demonstrate neuronal atrophy and astrocyte proliferation, and electrodiagnostic studies reveal a neurogenic pattern such as is seen in ALS.

PDB-like lesions are patchy with increased bone activity, cortical thickness and osteoclastogenesis on bone histology resembling the distribution in humans [31]. The *VCP*$^{R155H/+}$ mouse model, thus recapitulates human IBMPFD and may serve as a valuable tool for understanding the pathology of these diseases and for molecularly targeted therapeutic strategies, without any potential interference from overexpression of the mutant allele or from the Neomycin cassette.

MATERIALS AND METHODS

Ethics Statement

All experiments were done with the approval of the Institutional Animal Care and Use Committee (IACUC) of the University of California, Irvine (UCI) (IACUC Protocol #2007-2716), and in accordance with the guidelines established by the National Institutes of Health (NIH). Animals were housed in the animal facility of the University of California, Irvine, and were maintained under constant temperature (22°C) and humidity with a controlled 12:12-h light-dark cycle. Animals were observed throughout the entire experimental process in order to ameliorate any pain and suffering. Mice were euthanized by CO_2 inhalation followed by cervical dislocation.

Generation and Validation of the *VCP*$^{R155H/+}$ Mice

In order to generate a VCP disease mouse model, genomic *VCP* fragments with 7.9 kb of upstream homology sequence and 2.1 kb of downstream homology sequence were sub-cloned into a targeting vector. Site-directed mutagenesis using the Quick-Change XL Site-Directed Mutagenesis Kit (Stratagene, La Jolla, CA) was used to introduce the R to H mutation at amino acid position 155. The knock-in mouse model with the R155H *VCP* mutation was generated at InGenious Targeting Laboratory, Inc. (Stony Brook, NY) through

a Neomycin cassette insertion using 129/SvEv mice (Fig. 1A). The expression of mutant VCP was confirmed by RT-PCR using the following primers in the PCR reactions: Forward- 5′-CAC GGT GTT GCT AAA AGG AAA GAA AAG; Reverse- 3′-CTG AAG AAT CTC CAA ACG TCC TGT AGC, after the RT reactions with the reverse primer. These mice were back-crossed more than 6 times with the C57BL/6 strain before experiments were done to make sure that the majority (>98%) of the genetic background of generated mice was of C57BL/6 origin. The Neomycin cassette was deleted by crossing with the Flp deletion mouse model. Genotyping was performed by sending the mouse tail samples to Transnetyx Incorporation (Cordova, TN), and results were analyzed by our laboratory. The qRT-PCR analyses for expression of VCP showed no significant differences between WT and *VCP*$^{R155H/+}$ knock-in mouse quadriceps muscles (data not shown). Littermates were used in every experiment.

Weight, Motor Coordination, and Muscle Strength Measurement Studies

Weights of the *VCP*$^{R155H/+}$ and WT animals were measured on a weekly basis to follow body mass development. Motor coordination and fatigue were assessed by the Rotarod (Med Associates Inc., St. Albans, VT) accelerating speed analysis. The Rotarod test was performed for all existing mice at the age of 3 months (17 WT, 10 HET), 6 months (16 WT, 12 HET), 9 months (16 WT, 12 HET), 12 months (14 WT, 12 HET), and 15 months (14 WT, 12 HET), and 24 months (23 WT, 11 HET). Mice were placed on the Rotarod, which accelerates from 4 to 40 rpm in 5 minutes. Mice went through 3 trials with 45- to 60-minute inter-trial intervals on each of 2 consecutive days. The results were recorded as the time for the mouse to drop down from the Rotarod for the first time.

Muscle strength of the mouse forelimbs was measured using a Grip Strength Meter apparatus (TSE Systems Gmbh, Hamburg, Germany). Briefly, mice were held from the tip of the tail above the grid and gently lowered down until the front paws grasped the grid. Hind limbs were kept free from contact with the grid. The animal was brought to an almost horizontal position and pulled back gently, but steadily until the grip was released. The maximal force achieved by the animal was recorded. Each animal underwent 5 tests. The same cohort of mice used for the Rotarod test was also used for the grip strength studies until 15 months, and subsequent numbers of mice at different ages are: 18 months (6 WT, 5 HET), 24 months (18 WT, 8 HET), and 25-29 months old (6 WT, 4 HET), respectively. Statistical analyses were performed by Student *t*-test, and values were considered significant if $p<0.05$.

Immunohistochemical Analyses

Quadriceps muscles were flash frozen in isopentane cooled in liquid nitrogen, and brains from 15-, 19- and 24-month old mice (5 WT and 5 ~~KI~~ 2) were harvested and embedded in cryo-sectioning mounting media (Electron Microscopy Sciences, Hatfield, PA) and stored at −80°C before sectioning at 5-10μm. For immunohistochemical analyses, sections were incubated with TDP-43 (Abcam, Cambridge, MA), FK1 (Biomol, Plymouth Meeting, PA), VCP (Affinity BioReagents, Golden, CO), LC3-I/II (Novus Biologicals, Littleton, CO), and Neurofilament H non-phosphorylated (SMI-32) motor neuron marker (Sternberger Monoclonals, San Diego, CA) overnight in a humidified chamber. Subsequently, sections were washed with TBST (0.5%) and incubated with fluorescein-conjugated secondary antibodies (Sigma-Aldrich, St. Louis, MO) for 1 hour at room temperature and mounted with DAPI-containing mounting media (Vector Laboratories, Inc., Burlingame, CA). Sections were analyzed by fluorescence microscopy using an AxioVision image capture system (Carl Zeiss, Thornwood, NY). Additionally, Hematoxylin and Eosin (H&E) and Toluidine blue stains were performed using routine methods and analyzed by light microscopy (Carl Zeiss).

Cardiac perfusion was used for immunohistochemical characterization of the brain and spinal cord pathologies of our R155H heterozygote and WT mice. Animals were anesthetized with ketamine and perfused transcardially with Phosphate Buffered Saline (PBS), followed by 4% paraformaldehyde (PFA) for 10 minutes, after which spinal cords and brains were dissected. Tissues were subsequently incubated in 30% sucrose/PBS gradients for another 2 days and later processed for immunohistochemical analyses as described earlier.

Western Blotting

Quadriceps muscle samples from 15-, 19-, and 24-month-old wild-type and *VCP*$^{R155H/+}$ knock-in mice (5 wild-type and 5 knock-in mice from two litters) and 15 month-old wild-type and *VCP*$^{R155H/+}$ knock-in brain cortex samples were harvested and extracted using the NE-PER Nuclear and Cytoplasmic Extraction Kit (Thermo Scientific, Rockford, IL). Protein concentrations were determined using the Nanodrop according to the manufacturer's protocols. Equal amount of proteins were separated on Bis-Tris 4-12% NuPAGE gels using the Novex Mini Cell (Invitrogen Life Technologies, Carlsbad, CA) according to manufacturer's protocols. The expression levels of proteins were analyzed by Western blotting using TDP-43 (Abcam, Cambridge, MA), LC3-I/II (Novus Biologicals, Littleton, CO), and FK1 for ubiquitin (Biomol)-specific antibodies. Equal protein loading was confirmed by Beta actin antibody (Santa Cruz Biotechnology, Santa Cruz, CA) staining.

Apoptosis Analyses

Apoptosis in mouse quadriceps muscle tissue samples was analyzed by the DeadEnd Fluorometric TUNEL System (Promega, Madison, WI)and by the Colorimetric CaspACE-3 Assay System (Promega). For TUNEL analysis, muscle cryosections from 10-month old *VCP*$^{R155H/+}$ knock-in mice and WT littermates were stained as described previously [31].

MicroPET/CT Imaging and Bone Histomorphometry

For the microPET/CT scan, 16-month old mice were fasted for 24 hours, after which they were mildly anesthetized (2.5% isoflurane) and had 350μCi [^{18}F]-fluorodeoxyglucose (^{18}F-FDG) given via intraperitoneal injection (i.p.). The injected dose was measured by a dosimeter and was corrected for the residue of dose remained in the syringe. At 60 minutes post-intraperitoneal injection of [^{18}F]- fluorodeoxyglucose (^{18}F-FDG) (320–363 μCi), mice were placed under mild anesthesia, and a 40-min PET scan was performed on microPET/CT (Siemens Inc.). The transaxial FOV for Inveon PET is 10 cm, the axial FOV is 12.7 cm. The resolution in the center of transaxial FOV is 1.46 mm. Next, microCT scan was performed by scanning the mice with a large area CT camera that has a 30-40 micron high resolution, low noise, 14-bit X-ray imaging detector with 4096 × 4096 pixels. (Usable field of view for this configuration is 10 cm × 10 cm). The high performance 64-bit workstation controls the Inveon multimodality scanners and was also used for reconstruction of image data. The reconstructed microCT images were analyzed, and 3D trabecular structural parameters were determined using the Inveon Multimodality 3D Visualization software. The Bone volume/Total volume (BV/TV), Bone surface area/Bone volume (BS/BV), trabecular thickness (Tb. Th), trabecular space (Tb. Sp), trabecular number (Tb. N) and trabecular pattern factor (Tb. PF) were analyzed from 4 WT and 4 HET femurs (right and left femurs combined). Scans were performed at different ages of WT and VCP mutant animals.

RESULTS

Muscle weakness progresses in the *VCP*$^{R155H/+}$ knock-in mice typical of IBMPFD

Since patients typically demonstrate progressive muscle weakness in their 30s-40s we investigated the muscle strength and motor coordination and fatigue in the mice at 3-month intervals using grip strength and Rotarod analysis tests, respectively (Fig. 1B,C). Grip strength analyses in these knock-in mice showed a 4.0% decrease at 6 months (p=0.5), 12.7% at 9 months (p=0.008), 14.0% at 12 months (p=0.002), 16% at the age of 15 months (p=0.005), 21% at 19 months of age (p=0.001), 13.5% at 24 months of age (p=0.12), and 18.5% at 26 months of age (p=0.16) (Fig. 1B). Consistent with the grip strength, Rotarod analysis depicted 3% decreased muscle strength at the age of 6 months (p=0.54), 9.0% at 9 months (p=0.10), 13.7% at 12 months (p=0.10), 19.0% at 15 months (p=0.056), and 31% at 24 months (p=0.002) (Fig. 1C). The mice were unable to perform Rotarod testing after 24 months of age. There were no significant differences in mortality between KI and WT littermates when they were followed up to 28 months, which was evident by identical survival curves (data not shown). In contrast, the Neomycin cassette-containing mice developed muscle weakness earlier at 6-9 months of age as noted by grip strength and Rotarod testing compared to the equivalent age of 15 months for Rotarod testing and 9 months for grip strength in the *VCP*$^{R155H/+}$ mice; the latter pattern resembled that seen in patients.

Characterization of muscle pathology in *VCP*$^{R155H/+}$ knock-in mice reveals typical histopathological IBMPFD phenotype

H&E staining of quadriceps muscles demonstrated centrally located nuclei (Fig. 2A,B) variation in fiber size, and accumulation of rare vacuoles (Fig. 2C) in 15- and 24-month old *VCP*$^{R155H/+}$ knock-in mice. Six percent of *VCP*$^{R155H/+}$ muscle cells had inclusion bodies that were positive for the TDP-43 and ubiquitin-specific antibodies (Fig. 2D-I and Table 1). These inclusions were negative for the VCP antibody. Histological analysis of the gastrocnemius muscles from these *VCP*$^{R155H+}$ heterozygous mice revealed similar findings (provided as Supplemental Fig. 1). Western blotting analysis of 2 separate litter-matched wild-type and knock-in mice revealed that the mutant muscle had increased TDP-43 and ubiquitinated (FK1 marker) proteins (Fig. 2L). Electron microscopy imaging of the 19-month old *VCP*$^{R155H/+}$ knock-in mouse muscle showed extensive accumulation of abnormal mitochondria (black arrows) and vacuoles (white arrows) in the inter myofibrillar space as compared to the WT (Fig. 2J). Abnormal mitochondrial cristae structures (black arrows) were also observed in these VCP mutant mice (Fig. 2K). There was no significant heart pathology in the heterozygotes (provided as Supplemental Fig. 1).

Autophagy and apoptosis is increased in *VCP*$^{R155H/+}$ knock-in mice muscle

Autophagy is a process that degrades long-lived proteins and cytoplasmic components within vesicles which deliver the contents to the lysosome for degradation. Upon activation of autophagy, the 18 kDa cytosolic LC3 (LC3B-I) undergoes proteolytic cleavage followed by a lipid modification and is converted to the 16 kDa membrane-bound form (LC3B-II), which is specifically localized to the autophagosomal membranes. The conversion from LC3B-I to LC3B-II is used as a sensitive marker for autophagy in cells. Using myoblasts obtained from patients with VCP-associated IBM, we previously observed accumulation of enlarged vacuoles as well as other several cellular dysfunctions in patient myoblasts versus control myoblasts [7]. To analyze if autophagic processes were also disrupted in tissue in the knock-in mice, we analyzed the expression of the LC3B-II/I protein. Muscle cells from the VCP knock-in mice exhibited increased LC3-II staining, which was concentrated in the vesicular organelles throughout the cytoplasm as compared to WT littermates (Fig. 3A,B).

Western blot analysis of the knock-in *VCP*$^{R155H/+}$ quadriceps tissue lysates also demonstrated a significantly increased amount of LC3B-II (Fig. 3E).

Mutations in the VCP gene have been shown to trigger cell death with apoptosis, whereas expression of wild type protein has been suggested to have an anti-apoptotic effect [32-34]. TUNEL-staining of quadriceps sections showed an increased number of apoptotic nuclei which were centrally located in the knock-in muscle compared with WT [wild-type; 3.5% and *VCP*$^{R155H/+}$ knock-in 40% (15 month old) $p<0.05$ (Fig. 3C,D)]. There was increased caspase-3 specific activity in *VCP*$^{R155H/+}$ muscle as compared with WT littermates (Fig. 3F).

Bone pathology in *VCP*$^{R155H/+}$ knock-in animals resembles Paget Disease of Bone

To further characterize the bone pathology we analyzed bone morphology by micro CT imaging and histology. Gross micro CT images showed no obvious skeletal dysplasia of the knock-in *VCP*$^{R155H/+}$ mice (Fig. 4A,B). Close inspection of the long bones, however revealed lucencies of the proximal tibias (Fig. 4C,D). Bone morphometric analysis of the *VCP*$^{R155H/+}$ knock-in mice bones did not reveal significant differences of bone surface area/ bone volume (BS/BV), trabecular space (TbSp) trabecular pattern factor (TbPF) and cortical wall thickness (CTh) versus WT mice, except in the trabecular number (p=0.014) and cortical wall thickness (p=0.036) (Table 1).

To investigate bone turnover, *in vivo* imaging with $^{[18]}$F-fluoride positron emission tomography (PET) was carried out. Generally, PET uptake is more pronounced in regions of metabolic activity, as there is fluoride uptake on the bone surface when there is more new bone formation and higher blood flow to that area [35]. The PET scans showed increased fluoride uptake in 3 mice out of 5 heterozygotes scanned in the spine, tibia, or femur of 1 leg. There was increased fluoride uptake in the lumbar spine in the *VCP*$^{R155H/+}$ knock-in mice, suggestive of PDB, which was not observed in the WT animals (Fig. 4). Histopathology of the spine revealed that Paget-like lesions were increased in both number and size indicated by TRAP immunostaining of osteoclasts (data not shown).

Brain and spinal cord pathology in VCP$^{R155H/+}$ knock-in animals recapitulates ALS phenotype

Typical FTLD-U pathology has been reported in patient brains, including neocortex and limbic and subcortical nuclei. Histological analyses of the brain tissues from 15-month old mutant mice did not show any overt histological signs of degeneration in H&E staining. Immunohistochemical staining of the frontal cortex (Fig. 5) and hippocampus (data not shown), however, demonstrated an increase of TDP-43 and ubiquitin-positive inclusions. The TDP-43 inclusions showed increased cytoplasmic accumulation in the *VCP*$^{R155H/+}$ knock-in mouse brains, whereas the TDP-43 inclusions were localized to the nucleus in the cortex of control mice (Fig. 5A,B). Staining with ubiquitin and VCP demonstrated cytoplasmic inclusions in the frontal cortex in the mutant mice compared with the WT (Fig. 5C,D). Increased ubiquitin protein expression in the *VCP*$^{R155H/+}$ knock-in mice was also shown by western blot analysis (Fig. 5E).

Recently, studies have revealed *VCP* mutations are associated with typical ALS features in 2-3% of isolated familial ALS in addition to 10-15% frequency of ALS in VCP disease [10]. We studied the spinal cord pathology of 15-month old *VCP*$^{R155H/+}$ knock-in mice (Fig. 6). Toluidine blue staining revealed motor neurons and spinal cord injury in the 15-month old mutant mice (Fig. 6A,D). Increased TDP-43 expression levels were also observed in the anterior horn cells as compared with WT littermates (Fig. 6B,E). SMI-32 motor neuron

marker staining depicted normal morphology in the WT animals whereas *VCP*$^{R155H/+}$ knock-in mice exhibited fragmentation of cell body processes (Fig. 6C,F).

Electrodiagnostic studies reveal denervation in the *VCP*$^{R155H/+}$ knock-in mice

Electromyographic (EMG) evidence of widespread acute and chronic denervation was seen in *VCP*$^{R155H+}$ mice (average age 24.98 ± 0.41 months). These changes included a varying degree of abnormal spontaneous activity in the form of fibrillation and fasciculation potentials, and a distinct reduction in recruitment and interference patterns. Motor unit potential morphology was mixed, with both small amplitude as well as large amplitude potentials present in these muscles. Firing rates were generally decreased, again suggestive of a neurogenic pattern of activation rather than a myopathic pattern. The left hamstrings and medial gastrocnemius muscles of *VCP*$^{R155H+}$ heterozygous mice also showed complex repetitive discharges (CRD). All other muscles were normal. Interestingly, histological analysis of the gastrocnemius muscles from the *VCP*$^{R155H+}$ heterozygous mice revealed vacuoles and centrally located nuclei as compared with the WT animals, however there was no significant heart pathology (provided as Supplemental Fig. 1).

DISCUSSION

IBMPFD is a degenerative disease which affects various systems and is caused by *VCP* mutations. VCP is involved in a number of cellular functions, most of which are related to ubiquitin-proteasome-dependent proteolysis [20,36-39]. It is highly conserved in evolution, which suggests it has an essential role for normal cellular functions in both unicellular (yeast) and multi-cellular organisms [40-42]. The finding that inhibition of VCP expression promotes apoptosis [43], suggests that intact VCP is indispensable for normal development and cell survival. Additionally, our recent studies of patient myoblasts demonstrated accumulation of enlarged vacuoles [44]. Despite intense investigations, the critical disease mechanisms underlying VCP disease are yet to be clarified.

VCP-associated disease mouse models have been previously generated and characterized. The mouse system created by over-expression of the R155H mutation in mice using a muscle specific creatinine promoter created by Weihl et al (2007) revealed progressive muscle weakness beginning at the age of 6 months and muscle pathology, beginning at the age of 10 months, including variation in muscle fiber size, increase in endomysial connective tissue, small linear basophilic-rimmed cracks, and ubiquitin-positive sarcoplasmic and myonuclear vacuoles [29]. Custer et al. (2010) created transgenic mice that ubiquitously over-express mutant forms of VCP and exhibit typical inclusion body myopathy with muscle weakness and blue-rimmed vacuoles [45]. In our laboratory, Badadani et al (2010), generated and characterized the *VCP* knock-in mice with the R155H mutation including the Neomycin-cassette [31]. Typical characteristics of these mice included progressive muscle weakness as demonstrated by Rotarod and Grip Strength analysis, enlarged vacuoles and ubiquitin- and TDP-43-positive sarcoplasmic inclusion bodies in the quadriceps muscles. These mice also had disrupted autophagy, increased apoptosis processes, and seizures when compared with wild type animals. All of these murine models also demonstrated widespread TDP-43 brain pathology and Paget-like bone disease, all typical of human disease.

Our Neomycin cassette-free knock-in mouse system represents a unique opportunity for studying the mechanisms of VCP-associated disease in patients. Given this background, the findings of this study are unique in several respects. This model had muscle, bone, and brain pathology of VCP disease in aging mice with onset around 12-15 months of age. We assessed progression of disease in these mice up to 26 months of age. They exhibit muscle weakness, vacuoles and ubiquitin and TDP-43 positive inclusions in muscle fibers and brain,

typical ALS pathology of the spinal cord, and Paget-like bone changes on microPET/CT and histology. Electron microscopic analysis of 19-month old *VCP*$^{R155H/+}$ knock-in mouse muscle exhibits extensive accumulation of abnormal mitochondria and vacuoles in the inter-myofibrillar space suggestive of mitochondrial pathology. Mitochondria play an important role in several neurodegenerative diseases such as Parkinson disease and ALS. We have performed novelty toy tests on the *VCP*$^{R155H/+}$ knock-in and WT animals, but we have not observed any significant differences. Future studies will aim to perform additional behavioral studies to detect any abnormalities and to understand the molecular mechanism of mitochondrial dysfunction in the pathogenesis of VCP-associated disease. Collectively, these findings suggest that our mouse model has a comparable disease progression and pathology as that seen in patients who develop late onset muscle weakness at a mean age of 42 years [1]46-47. Thus, the *VCP*$^{R155H/+}$ mouse represents an important and faithful experimental model for probing the underlying mechanisms responsible for these unique diseases and novel treatments.

Frontotemporal dementia is a degenerative condition of the brain which primarily affects the frontal and anterior temporal lobes at a mean age of 57 years [15]. No short-term memory deficiencies were observed in the Neomycin cassette-free *VCP*$^{R155H/+}$ knock-in mice studied here. We observed accumulation of TDP-43-, ubiquitin-, and VCP-positive inclusions in the 15-month and older knock-in brains, and not in 10-month old brain, mimicking the delayed development of FTD in patients. TDP-43 inclusions in the *VCP*$^{R155H/+}$ knock-in mouse brains were cytoplasmic, in contrast to the nuclear localization in the cortex and hippocampus of control mice [48].

ALS associated with motor neuron degeneration in the brain and spinal cord caused by mutations in superoxide dismutase 1 (SOD1), TDP-43 and fused in sarcoma (FUS), optineurin and VCP [9]49-51 accounts for approximately 10-15% of familial ALS cases. The similar TDP-43 pathology in the brain and spinal cord suggested shared pathogenetic mechanisms with ALS. Furthermore, mutations in *UBQLN2*, which encode the ubiquitin-like protein Ubiquilin 2, a regulator of degradation of ubiquitinated proteins, have been identified as the cause of dominant X-linked juvenile and adult-onset ALS and ALS/dementia. [52] This underscores the importance of the ubiquitin-proteasome pathway in the pathogenesis of VCP and ALS. Most recently, the pathological hexanucleotide repeat expansion in the C9*orf*72 gene has been associated with the cause of both chromosome 9p21-linked frontotemporal lobar degeneration (FTLD) and ALS [53-56]. The GGGGCC repeat expansions in these patient cohorts resulted in high mutation frequencies and may provide evidence for the biological association between these neurodegenerative diseases. Future studies may identificy new genes and biological/molecular mechanisms responsible for these phenotypes and ultimately therapeutic approaches to treat these progressive neurodegenerative disorders.

Autophagy is a process that functions as a stress response that is upregulated by starvation, oxidative stress, or other harmful conditions. It plays a role in programmed cell death and possesses important housekeeping and quality control functions that contribute to health and longevity (for review, see [57-60]). Danon disease is an example of a human myopathy that is characterized by accumulation of autophagic vacuoles in the heart and skeletal muscle [61]. A mouse model for Danon disease exhibits similar histological and phenotypical features to human patients. There are massive accumulation of autophagic vacuoles in several tissues, including skeletal muscle and heart [62]. Mitochondria are a main target for autophagic degradation in muscle diseases resulting in reduced mitochondrial function, which leads to defective energy metabolism and reduced contractility [63]. Therefore, increased autophagosome formation as exhibited by LC3-II accumulation and muscle weakness in both our *VCP*$^{R155H/+}$ knock-in mice and patients, is consistent with other myopathic

conditions and suggests a common pathogenesis. The histology in both *VCP*$^{R155H/+}$ knock-in mice and patients indicate not only induction of autophagy, but also disruption of the autophagic maturation process. The current hypothesis is that immature autophagosomes accumulate in tissues secondary to impaired lysosome-autophagosome fusion and thus further contribute to tissue pathology. Our recent studies in myoblasts from IBMPFD patients show increased apoptosis when they are analyzed by caspase-3 assays and TUNEL staining, and there is increased autophagy [44].

Histochemical stains of vertebral bone revealed increased osteoclastic activity typical of Paget disease. Giant osteoclast formation resembles the human Pagetic osteoclast phenotype. PDB is characterized by abnormal bone remodeling, osteolytic lesions, bone deformities and pathologic fractures. An initial surge of osteoclastic activity leads to focalized resorption of bone, followed shortly thereafter, by osteoblast hyperactivity. The osteoblasts are normal morphologically, but they deposit new bone in a disordered manner to result in the Pagetic lesions. The new disorganized bone is of poor quality and leads to bowing and occasionally fractures. In the more advanced stages of Paget disease, the rapid bone formation predominates. The lesions become sclerotic, and bone marrow is replaced with vascular and fibrous tissue and increased bone thickness. Recent studies have demonstrated that 10% of patients with sporadic PDB and 50% of familial PDB have *Sequestosome 1* (*SQSTM1*) gene mutations, which encodes p62 and has an important role in autophagy. The *SQSTM/P62 P394L* mutant mice [64] revealed focal osteolytic lesions on hind limbs by micro CT pathology which resembles the lesions seen in our new Paget disease-like mouse model. Several studies have shown PET imaging to be a good method to test for PDB [65-67], although it is not a conclusive test. It is interesting to note that the spine, particularly the lumbar region, is the second most commonly affected site (53%) after the pelvis (70%) in PDB patients [68-70]. This strengthens the argument that what we are seeing in the *VCP*$^{R155H/+}$ mice is PDB, thus they also promise to be a good model for PDB.

We propose that the VCP$^{R155H/+}$ knock-in mouse represents an excellent model for VCP-associated myopathy, PDB, and ALS; these diseases share a common pathogenic mechanism associated with defects in the protein degradation pathway. Thus, the neomycin cassette-free *VCP*$^{R155H/+}$ knock-in mouse can be exploited for the development of novel strategies and treatments without potential interference from the Neomycin cassette.

Supplementary Material

Refer to Web version on PubMed Central for supplementary material.

Acknowledgments

We thank Drs. Cristian Constantinescu and Mohammad Reza Mirbolooki for technical assistance with the MicroCT. We thank Michael Baker and Dr. Masashi Kitazawa for technical assistance, helpful discussion and critical reading of the manuscript. We thank Dr. Ronald Kim for his expertise in the electron microscopy analysis. Funding for this study was provided by NIH grants AR050236 and Muscular Dystrophy Association MDA175682 (VEK) and NS36548 (JHW).

Abbreviations

(ALS)	Amyotrophic Lateral Sclerosis
(EMG)	Electromyography
(IBMPFD)	Inclusion Body Myopathy, Paget Disease of Bone, Frontotemporal Dementia

(LC3I/II)	Light Chain 3
(P62/SQSTM)	P62 Sequestesome
(TDP-43)	TAR-DNA Binding Protein-43
(VCP)	Valosin Containing Protein

REFERENCES

1. Kimonis VE, Kovach MJ, Waggoner B, Leal S, Salam A, Rimer L, et al. Clinical and molecular studies in a unique family with autosomal dominant limb-girdle muscular dystrophy and Paget disease of bone. Genet Med. 2000; 2(4):232–41. [PubMed: 11252708]
2. Watts GD, Wymer J, Kovach MJ, Mehta SG, Mumm S, Darvish D, et al. Inclusion body myopathy associated with Paget disease of bone and frontotemporal dementia is caused by mutant valosin-containing protein. Nature genetics. 2004; 36(4):377–81. [PubMed: 15034582]
3. Kimonis VE, Mehta SG, Fulchiero EC, Thomasova D, Pasquali M, Boycott K, et al. Clinical studies in familial VCP myopathy associated with Paget disease of bone and frontotemporal dementia. Am J Med Genet A. 2008; 146A(6):745–57. [PubMed: 18260132]
4. Watts GD, Thorne M, Kovach MJ, Pestronk A, Kimonis VE. Clinical and genetic heterogeneity in chromosome 9p associated hereditary inclusion body myopathy: exclusion of GNE and three other candidate genes. Neuromuscul Disord. 2003; 13(7-8):559–67. [PubMed: 12921793]
5. Kimonis VE, Fulchiero E, Vesa J, Watts G. VCP disease associated with myopathy, Paget disease of bone and frontotemporal dementia: review of a unique disorder. Biochimica et biophysica acta. 2008; 1782(12):744–8. [PubMed: 18845250]
6. Weihl CCTP, Miller SE, Watts G, Smith C, Forman M, Hanson PI, Kimonis V, Pestronk A. TDP-43 accumulation in IBM muscle suggests a common pathogenic mechanism with Frontotemporal dementia. 2008
7. Vesa J, Su H, Watts GD, Krause S, Walter MC, Martin B, et al. Valosin containing protein associated inclusion body myopathy: abnormal vacuolization, autophagy and cell fusion in myoblasts. Neuromuscul Disord. 2009; 19(11):766–72. [PubMed: 19828315]
8. Shaw CE. Capturing VCP: another molecular piece in the ALS jigsaw puzzle. Neuron. 2010; 68(5): 812–4. [PubMed: 21144996]
9. Leigh PN, Wijesekera LC. Motor neuron disease: focusing the mind on ALS: updated practice parameters. Nat Rev Neurol. 2010; 6(4):191–2. [PubMed: 20379204]
10. Johnson JO, Mandrioli J, Benatar M, Abramzon Y, Van Deerlin VM, Trojanowski JQ, et al. Exome sequencing reveals VCP mutations as a cause of familial ALS. Neuron. 2010; 68(5):857–64. [PubMed: 21145000]
11. Abramzon Y, Johnson JO, Scholz SW, Taylor JP, Brunetti M, Calvo A, et al. Valosin-containing protein (VCP) mutations in sporadic amyotrophic lateral sclerosis. Neurobiology of aging. 2012 [PubMed: 22572540]
12. Tiloca C, Ratti A, Pensato V, Castucci A, Soraru G, Del Bo R, et al. Mutational analysis of VCP gene in familial amyotrophic lateral sclerosis. Neurobiology of aging. 2012; 33(3):630 e1–2.
13. Williams KL, Solski JA, Nicholson GA, Blair IP. Mutation analysis of VCP in familial and sporadic amyotrophic lateral sclerosis. Neurobiology of aging. 2011
14. Farpour F, Tehranzadeh J, Donkervoort S, Smith C, Martin B, Vanjara P, et al. Radiological features of Paget disease of bone associated with VCP myopathy. Skeletal radiology. 2011 [PubMed: 21643886]
15. Kimonis VE, Mehta SG, Fulchiero EC, Thomasova D, Pasquali M, Boycott K, et al. Clinical studies in familial VCP myopathy associated with Paget disease of bone and frontotemporal dementia. Am J Med Genet A. 2008; 146(6):745–57.
16. Arnold SE, Han LY, Clark CM, Grossman M, Trojanowski JQ. Quantitative neurohistological features of frontotemporal degeneration. Neurobiology of aging. 2000; 21(6):913–9. [PubMed: 11124442]

17. Turner RS, Kenyon LC, Trojanowski JQ, Gonatas N, Grossman M. Clinical, neuroimaging, and pathologic features of progressive nonfluent aphasia. Annals of neurology. 1996; 39(2):166–73. [PubMed: 8967747]

18. Zhukareva V, Vogelsberg-Ragaglia V, Van Deerlin VM, Bruce J, Shuck T, Grossman M, et al. Loss of brain tau defines novel sporadic and familial tauopathies with frontotemporal dementia. Annals of neurology. 2001; 49(2):165–75. [PubMed: 11220736]

19. DeLaBarre B, Brunger AT. Complete structure of p97/valosin-containing protein reveals communication between nucleotide domains. Nature structural biology. 2003; 10(10):856–63. [PubMed: 12949490]

20. Dai RM, Li CC. Valosin-containing protein is a multi-ubiquitin chain-targeting factor required in ubiquitin-proteasome degradation. Nature cell biology. 2001; 3(8):740–4. [PubMed: 11483959]

21. Ju JS, Fuentealba RA, Miller SE, Jackson E, Piwnica-Worms D, Baloh RH, et al. Valosin-containing protein (VCP) is required for autophagy and is disrupted in VCP disease. The Journal of cell biology. 2009; 187(6):875–88. [PubMed: 20008565]

22. Weihl CC, Pestronk A, Kimonis VE. Valosin-containing protein disease: inclusion body myopathy with Paget's disease of the bone and fronto-temporal dementia. Neuromuscul Disord. 2009; 19(5): 308–15. [PubMed: 19380227]

23. Tang WK, Li D, Li CC, Esser L, Dai R, Guo L, et al. A novel ATP-dependent conformation in p97 N-D1 fragment revealed by crystal structures of disease-related mutants. The EMBO journal. 2010; 29(13):2217–29. [PubMed: 20512113]

24. Ju JS, Weihl CC. Inclusion body myopathy, Paget's disease of the bone and fronto-temporal dementia: a disorder of autophagy. Human molecular genetics. 2010; 19(R1):R38–45. [PubMed: 20410287]

25. Hubbers CU, Clemen CS, Kesper K, Boddrich A, Hofmann A, Kamarainen O, et al. Pathological consequences of VCP mutations on human striated muscle. Brain. 2007; 130(Pt 2):381–93. [PubMed: 16984901]

26. Nalbandian A, Donkervoort S, Dec E, Badadani M, Katheria V, Rana P, et al. The Multiple Faces of Valosin-Containing Protein-Associated Diseases: Inclusion Body Myopathy with Paget's Disease of Bone, Frontotemporal Dementia, and Amyotrophic Lateral Sclerosis. J Mol Neurosci. 2011 [PubMed: 21892620]

27. Muller JM, Meyer HH, Ruhrberg C, Stamp GW, Warren G, Shima DT. The mouse p97 (CDC48) gene. Genomic structure, definition of transcriptional regulatory sequences, gene expression, and characterization of a pseudogene. The Journal of biological chemistry. 1999; 274(15):10154–62. [PubMed: 10187799]

28. Muller JM, Deinhardt K, Rosewell I, Warren G, Shima DT. Targeted deletion of p97 (VCP/CDC48) in mouse results in early embryonic lethality. Biochemical and biophysical research communications. 2007; 354(2):459–65. [PubMed: 17239345]

29. Weihl CC, Miller SE, Hanson PI, Pestronk A. Transgenic expression of inclusion body myopathy associated mutant p97/VCP causes weakness and ubiquitinated protein inclusions in mice. Human molecular genetics. 2007; 16(8):919–28. [PubMed: 17329348]

30. Custer SK, Neumann M, Lu H, Wright AC, Taylor JP. Transgenic mice expressing mutant forms VCP/p97 recapitulate the full spectrum of IBMPFD including degeneration in muscle, brain and bone. Human molecular genetics. 2010; 19(9):1741–55. [PubMed: 20147319]

31. Badadani M, Nalbandian A, Watts GD, Vesa J, Kitazawa M, Su H, et al. VCP associated inclusion body myopathy and paget disease of bone knock-in mouse model exhibits tissue pathology typical of human disease. PloS one. 2010; 5(10) [PubMed: 20957154]

32. Hirabayashi M, Inoue K, Tanaka K, Nakadate K, Ohsawa Y, Kamei Y, et al. VCP/p97 in abnormal protein aggregates, cytoplasmic vacuoles, and cell death, phenotypes relevant to neurodegeneration. Cell death and differentiation. 2001; 8(10):977–84. [PubMed: 11598795]

33. Kobayashi T, Tanaka K, Inoue K, Kakizuka A. Functional ATPase activity of p97/valosin-containing protein (VCP) is required for the quality control of endoplasmic reticulum in neuronally differentiated mammalian PC12 cells. The Journal of biological chemistry. 2002; 277(49):47358–65. [PubMed: 12351637]

34. Shirogane T, Fukada T, Muller JM, Shima DT, Hibi M, Hirano T. Synergistic roles for Pim-1 and c-Myc in STAT3-mediated cell cycle progression and antiapoptosis. Immunity. 1999; 11(6):709–19. [PubMed: 10626893]
35. Cook GJ, Blake GM, Marsden PK, Cronin B, Fogelman I. Quantification of skeletal kinetic indices in Paget's disease using dynamic 18F-fluoride positron emission tomography. J Bone Miner Res. 2002; 17(5):854–9. [PubMed: 12009016]
36. Bays NW, Hampton RY. Cdc48-Ufd1-Npl4: stuck in the middle with Ub. Curr Biol. 2002; 12(10):R366–71. [PubMed: 12015140]
37. Fu X, Ng C, Feng D, Liang C. Cdc48p is required for the cell cycle commitment point at Start via degradation of the G1-CDK inhibitor Far1p. The Journal of cell biology. 2003; 163(1):21–6. [PubMed: 14557244]
38. Richly H, Rape M, Braun S, Rumpf S, Hoege C, Jentsch S. A series of ubiquitin binding factors connects CDC48/p97 to substrate multiubiquitylation and proteasomal targeting. Cell. 2005; 120(1):73–84. [PubMed: 15652483]
39. Ye Y, Meyer HH, Rapoport TA. The AAA ATPase Cdc48/p97 and its partners transport proteins from the ER into the cytosol. Nature. 2001; 414(6864):652–6. [PubMed: 11740563]
40. Frohlich KU, Fries HW, Rudiger M, Erdmann R, Botstein D, Mecke D. Yeast cell cycle protein CDC48p shows full-length homology to the mammalian protein VCP and is a member of a protein family involved in secretion, peroxisome formation, and gene expression. The Journal of cell biology. 1991; 114(3):443–53. [PubMed: 1860879]
41. Lamb JR, Fu V, Wirtz E, Bangs JD. Functional analysis of the trypanosomal AAA protein TbVCP with trans-dominant ATP hydrolysis mutants. The Journal of biological chemistry. 2001; 276(24): 21512–20. [PubMed: 11279035]
42. Leon A, McKearin D. Identification of TER94, an AAA ATPase protein, as a Bam-dependent component of the Drosophila fusome. Molecular biology of the cell. 1999; 10(11):3825–34. [PubMed: 10564274]
43. Wojcik C, Yano M, DeMartino GN. RNA interference of valosin-containing protein (VCP/p97) reveals multiple cellular roles linked to ubiquitin/proteasome-dependent proteolysis. Journal of cell science. 2004; 117(Pt 2):281–92. [PubMed: 14657277]
44. Vesa J, Su H, Fan W, Watts GD, Krause S, Walter MC, et al. Mechanisms of p97/VCP associated Inclusion Body and Vacuolar Myopathy: Studies in Human Myoblasts. 2009 Submitted.
45. Custer SK, Neumann M, Lu H, Wright AC, Taylor JP. Transgenic mice expressing mutant forms VCP/p97 recapitulate the full spectrum of IBMPFD including degeneration in muscle, brain and bone. Human molecular genetics. 2010 [PubMed: 20147319]
46. Kimonis VE, Watts GD. Autosomal dominant inclusion body myopathy, Paget disease of bone, and frontotemporal dementia. Alzheimer disease and associated disorders. 2005; 19(Suppl 1):S44–7. [PubMed: 16317258]
47. Kovach MJ, Waggoner B, Leal SM, Gelber D, Khardori R, Levenstien MA, et al. Clinical delineation and localization to chromosome 9p13.3-p12 of a unique dominant disorder in four families: hereditary inclusion body myopathy, Paget disease of bone, and frontotemporal dementia. Molecular genetics and metabolism. 2001; 74(4):458–75. [PubMed: 11749051]
48. Neumann M, Mackenzie IR, Cairns NJ, Boyer PJ, Markesbery WR, Smith CD, et al. TDP-43 in the ubiquitin pathology of frontotemporal dementia with VCP gene mutations. Journal of neuropathology and experimental neurology. 2007; 66(2):152–7. [PubMed: 17279000]
49. Kakizuka A. Roles of VCP in human neurodegenerative disorders. Biochemical Society transactions. 2008; 36(Pt 1):105–8. [PubMed: 18208395]
50. Mizuno Y, Hori S, Kakizuka A, Okamoto K. Vacuole-creating protein in neurodegenerative diseases in humans. Neuroscience letters. 2003; 343(2):77–80. [PubMed: 12759168]
51. Guyant-Marechal L, Laquerriere A, Duyckaerts C, Dumanchin C, Bou J, Dugny F, et al. Valosin-containing protein gene mutations: clinical and neuropathologic features. Neurology. 2006; 67(4): 644–51. [PubMed: 16790606]
52. Deng HX, Chen W, Hong ST, Boycott KM, Gorrie GH, Siddique N, et al. Mutations in UBQLN2 cause dominant X-linked juvenile and adult-onset ALS and ALS/dementia. Nature. 2011; 477(7363):211–5. [PubMed: 21857683]

53. DeJesus-Hernandez M, Desaro P, Johnston A, Ross OA, Wszolek ZK, Ertekin-Taner N, et al. Novel p.Ile151Val mutation in VCP in a patient of African American descent with sporadic ALS. Neurology. 2011; 77(11):1102–3. [PubMed: 21880997]
54. Gijselinck I, Van Langenhove T, van der Zee J, Sleegers K, Philtjens S, Kleinberger G, et al. A C9orf72 promoter repeat expansion in a Flanders-Belgian cohort with disorders of the frontotemporal lobar degeneration-amyotrophic lateral sclerosis spectrum: a gene identification study. Lancet Neurol. 2012; 11(1):54–65. [PubMed: 22154785]
55. Renton AE, Majounie E, Waite A, Simon-Sanchez J, Rollinson S, Gibbs JR, et al. A hexanucleotide repeat expansion in C9ORF72 is the cause of chromosome 9p21-linked ALS-FTD. Neuron. 2011; 72(2):257–68. [PubMed: 21944779]
56. van Langenhove T, van der Zee J, van Broeckhoven C. The molecular basis of the frontotemporal lobar degeneration-amyotrophic lateral sclerosis spectrum. Ann Med. 2012 [PubMed: 22420316]
57. Bergamini E, Cavallini G, Donati A, Gori Z. The role of autophagy in aging: its essential part in the anti-aging mechanism of caloric restriction. Annals of the New York Academy of Sciences. 2007; 1114:69–78. [PubMed: 17934054]
58. Eskelinen EL. Maturation of autophagic vacuoles in Mammalian cells. Autophagy. 2005; 1(1):1–10. [PubMed: 16874026]
59. Galluzzi L, Vicencio JM, Kepp O, Tasdemir E, Maiuri MC, Kroemer G. To die or not to die: that is the autophagic question. Current molecular medicine. 2008; 8(2):78–91. [PubMed: 18336289]
60. Scarlatti F, Granata R, Meijer AJ, Codogno P. Does autophagy have a license to kill mammalian cells? Cell death and differentiation. 2009; 16(1):12–20. [PubMed: 18600232]
61. Nishino I. Autophagic vacuolar myopathies. Current neurology and neuroscience reports. 2003; 3(1):64–9. [PubMed: 12507414]
62. Tanaka Y, Guhde G, Suter A, Eskelinen EL, Hartmann D, Lullmann-Rauch R, et al. Accumulation of autophagic vacuoles and cardiomyopathy in LAMP-2-deficient mice. Nature. 2000; 406(6798): 902–6. [PubMed: 10972293]
63. Stypmann J, Janssen PM, Prestle J, Engelen MA, Kogler H, Lullmann-Rauch R, et al. LAMP-2 deficient mice show depressed cardiac contractile function without significant changes in calcium handling. Basic research in cardiology. 2006; 101(4):281–91. [PubMed: 16604439]
64. Daroszewska A, van 't Hof RJ, Rojas JA, Layfield R, Landao-Basonga E, Rose L, et al. A point mutation in the ubiquitin-associated domain of SQSMT1 is sufficient to cause a Paget's disease-like disorder in mice. Human molecular genetics. 2011; 20(14):2734–44. [PubMed: 21515589]
65. Dell'Atti C, Cassar-Pullicino VN, Lalam RK, Tins BJ, Tyrrell PN. The spine in Paget's disease. Skeletal radiology. 2007; 36(7):609–26. [PubMed: 17410356]
66. Nguyen BD, Ram PC, Roarke MC. PET/CT imaging of metastatic deposit in vertebral Paget's disease. Clinical nuclear medicine. 2005; 30(5):359–60. [PubMed: 15827416]
67. Niederkohr RD, Gambhir SS. F-18 FDG PET/CT imaging of extramammary Paget disease of the perianal region. Clinical nuclear medicine. 2006; 31(9):561–3. [PubMed: 16921286]
68. Altman RD, Brown M, Gargano F. Low back pain in Paget's disease of bone. Clinical orthopaedics and related research. 1987; (217):152–61. [PubMed: 2951047]
69. Langston AL, Ralston SH. Management of Paget's disease of bone. Rheumatology (Oxford, England). 2004; 43(8):955–9.
70. Meunier PJ, Salson C, Mathieu L, Chapuy MC, Delmas P, Alexandre C, et al. Skeletal distribution and biochemical parameters of Paget's disease. Clinical orthopaedics and related research. 1987; (217):37–44. [PubMed: 3103964]

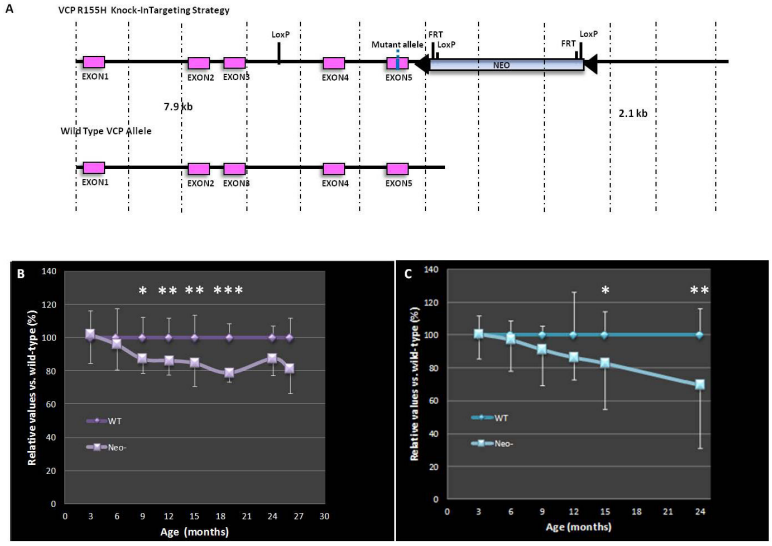

FIGURE 1. Generation of the *VCP*$^{R155H/+}$ knock-in mice and progression of muscle weakness

(A) Drawing of the R155H targeting strategy of the knock-in allele (top) and the wild type allele (below). The alleles depict the localization of exons 1-5, and the 5′ (7.9kb) and 3′ (2.1kb) targeting sequences indicated by dashed lines. The Neomycin-cassette is marked by Neo, flanked by FRT sites and restriction enzymes. (B) Muscle strength impairment observed by grip strength meter in knock-in mice as compared with littermates. (C) Physical performance demonstrated a decline by Rotarod analysis in the *VCP* knock-in mice as compared with littermates. Animal ages (months) (X axis) and relative values versus wild-type littermates (Y axis). Statistically significant *p<0.05, **p<0.005, and ***p<0.001 values denoted.

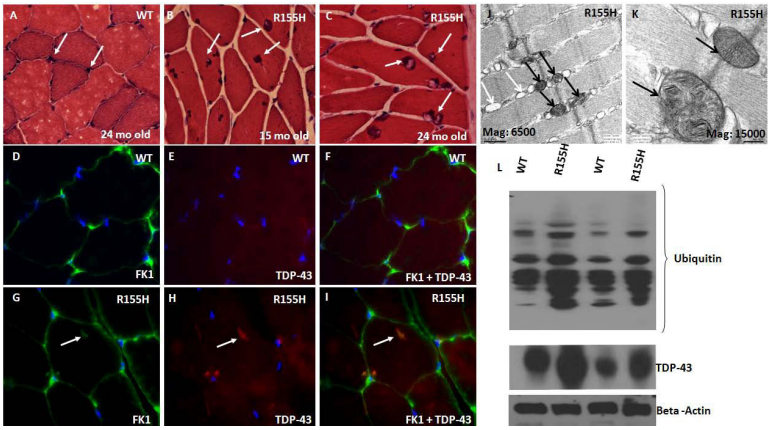

FIGURE 2. Histological analysis of the *VCP*$^{R155H/+}$ mouse quadriceps muscles

(A) H&E staining of quadriceps muscle from 24-month-old wild-type (nuclei depicted by arrows) and (B, C) 15- and 24-month old *VCP*$^{R155H/+}$ knock-in mice. (B) Centrally located nuclei are shown by arrows (C) Enlarged vacuoles in the mutant quadriceps (Magnification: 630X). Quadriceps muscles from (D-F) wild-type and (G-I) *VCP*$^{R155H/+}$ knock-in mice were stained with ubiquitin-specific FK1 antibody and a TDP-43-specific antibody and then double-stained with both antibodies. (I) Overlay of ubiquitin and TDP-43-positive cytoplasmic inclusion bodies as shown by arrow. Nuclei were stained with DAPI (Magnification: 630X). (J) Electron microscopy image of 19-month old *VCP*$^{R155H/+}$ knock-in mouse muscle showing extensive accumulation of abnormal mitochondria (black arrows) and vacuoles (white arrows) in the inter-myofibrillar space (Magnification 6500X) and (K) abnormal mitochondrial cristae structure (black arrows) (Magnification 15000X). (L) Proteins were harvested from the quadriceps muscle of wild-type and knock-in mice and analyzed by Western blotting using ubiquitin/FK1 (upper panel) and TDP-43 (lower panel) antibodies. Each membrane was reprobed with β-actin to confirm equal protein loading in each lane.

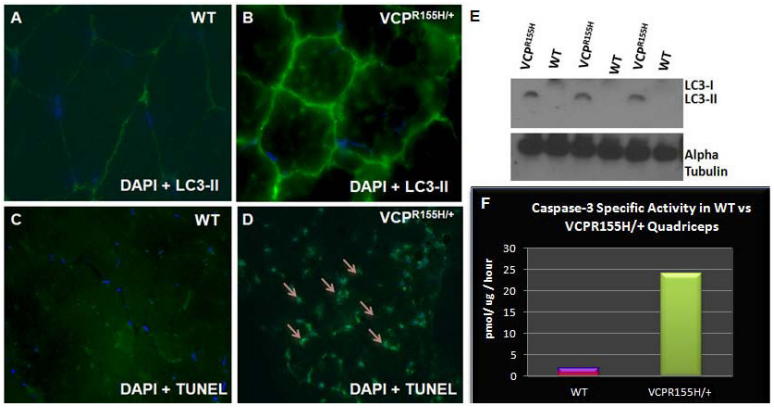

FIGURE 3. LC3-II staining of WT and *VCP*$^{R155H/+}$ knock-in mouse quadriceps muscle

Quadriceps muscles from (A) wild-type and (B) R155H knock-in mice were stained with an LC3-II-specific antibody. (B) LC3-positive vesicles are shown by arrows suggestive of increased autophagy. Nuclei were stained blue with DAPI. (C,D) DAPI and TUNEL staining of the quadriceps from WT and *VCP*$^{R155H/+}$ mouse models. (Magnification: 630X). (D) Apoptotic nuclei of the mutant mice are shown by white arrows. (E) LC3 expression was measured from the quadriceps muscle lysates of WT and R155H knock-in mice by western blotting. (Magnification: 400X). Wild-type and knock-in samples are from 3 different litters. (F) Caspase-3 specific activity level was measured from *VCP*$^{R155H/+}$ knock-in and WT mouse quadriceps muscle lysates. Specific activities are shown on the Y axis and mouse genotypes on the X axis.

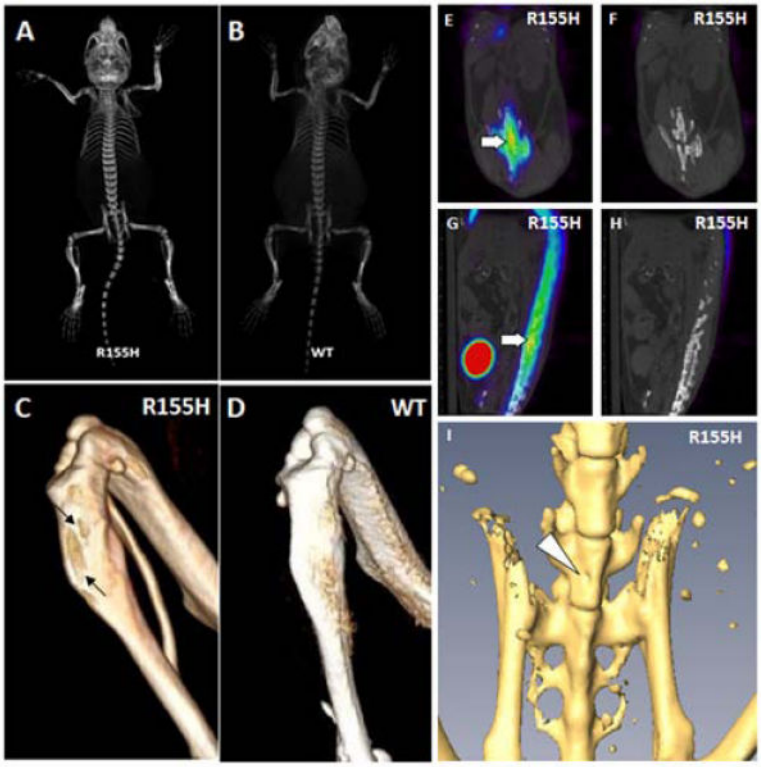

FIGURE 4. Pet and Micro CT images of bone in WT and *VCP*$^{R155H/+}$ knock-in mice

No obvious structural differences between the (A) R155H mutant and the (B) WT were seen of the CT images. The tibiae however showed abnormal architecture in the (C) R155H mutant highlighted with black arrows. (D) None can be seen in the WT. (E-H) *In vivo* imaging with microPET/CT demonstrates area of bone turnover. Sagittal view (E) with and (F) without the microPET image superimposed on the corresponding microCT image. Coronal view (G) with and (H) without overlaid images. Arrows indicate areas of increased bone turnover. (I) Micro CT reconstruction of an animal with PDB revealing the Pagetic lesion as cortical pitting (as shown by arrowhead).

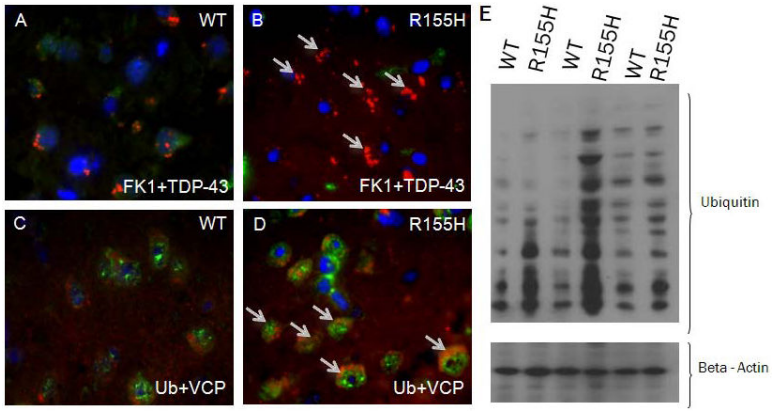

FIGURE 5. Immunohistochemical staining of the WT and *VCP*$^{R155H/+}$ knock-in mouse brain

cortexBrain cortex from (A) WT and (B) R155H knock-in mice were double stained with ubiquitin-specific FK1 antibody (TRITC-labeled) and TDP-43-specific antibody (FITC-labeled). Nuclei were stained with DAPI. Ubiquitin and TDP43-positive cytoplasmic inclusion bodies shown by arrows are predominantly nuclear in the WT and cytoplasmic in the mutant mice. Brain cortex from (C) WT mice and (D) *VCP*$^{R155H/+}$ knock-in mice were stained with ubiquitin and VCP antibodies. Mutant knock-in mice showed increased expression of ubiquitin as compared to WT, whereas there was no difference in VCP expression in either mutant or WT littermates (Magnification: 630X). (E) Proteins were harvested from the quadriceps muscle of wild-type and knock-in mice and analyzed by Western blotting using ubiquitin/FK1 antibodies. The membrane was reprobed with actin to confirm equal protein loading in each lane. Wild-type and knock-in samples are from 2 separate litters (indicated above the figure).

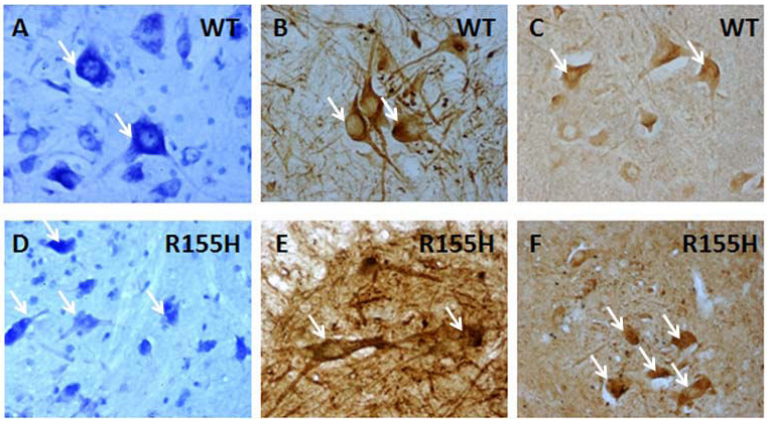

FIGURE 6. Histological analyses of spinal cord in WT and *VCP*$^{R155H/+}$ mouse model

(A,D) Toluidine Blue staining demonstrates degenerating motor neuron cells (indicated by arrows) in 15-month old R155H mutant mouse (20 uM sections) motor neurons versus WT mice (A, D) (Magnification 400X). (B) Neurofilament H Non-Phosphorylated (SMI-32) motor neuron marker staining shows normal morphology in the WT animals, whereas (E) *VCP*$^{R155H/+}$ mice exhibit fragmentation of cell body processes (indicated by arrows). (C) Normal TDP-43 expression pattern in WT and (F) high levels of TDP-43 expression in cytoplasm of VCP$^{R155H/+}$ knock-in mice (indicated by arrows).

Table 1

Bone morphometric analysis in WT and VCP$^{R155H/+}$ knock-in mouse model

Analysis of bone morphometrics including bone volume, bone surface area, trabecular thickness, number, spacing,and pattern factor, and cortical wall thickness in WT and VCP$^{R155H/+}$ animals. Statistically significant differences were identified in the trabecular number and cortical wall thickness of femurs of mice.

Parameter	Wild Type Mice	VCP$^{R155H/+}$ Mice
Bone Volume/Total Volume (BV/TV)	0.666 ± 0.042	0.583 ± .079 p=0.23
Bone Surface Area/Bone Volume (BS/BV)	18 ± 0.73	19.4 ± 3.24 p=0.32
Trabecular Thickness (TbTh)	0.111 ± 0.0045	0.105 ± .0162 p=0.088
Trabecular Number (TbN)	6.00 ± 0.324	5.57 ± 0.591 p=0.014*
Trabecular Spacing (TbSp)	0.05613 ± 0.0097	0.07588 ± 0.0182 p=0.93
Trabecular Pattern Factor (TbPF)	3.36 ± 1.03	3.42 ± 1.73 p=0.93
Cortical Wall Thickness (CTh)	1.65 ± 0.418	2.1 ± 0.33 p=0.036*

Statistically significant data are represented by

* $p<0.05$.